Ferroelectric behavior of orthogonal smectic phase made of bent-core molecules

Lingfeng Guo, Ewa Gorecka, Damian Pociecha, Nataša Vaupotič, Mojca Čepič, R. Amaranatha Reddy, Kristina Gornik, Fumito Araoka, Noel A. Clark, David M. Walba, Ken Ishikawa, and Hideo Takezoe

Phys. Rev. E **84**, 031706 — Published 21 September 2011

DOI: 10.1103/PhysRevE.84.031706

Ferroelectric behavior of orthogonal smectic phase made of bent-core molecules

Lingfeng Guo,[1] Ewa Gorecka,[2] Damian Pociecha,[2] Nataša Vaupotič,[3,4] Mojca Čepič,[4,5] R. Amaranatha Reddy,[6] Kristina Gornik,[3,5] Fumito Araoka,[1] Noel A. Clark,[7] David M. Walba,[6] Ken Ishikawa,[1] Hideo Takezoe*[1]

[1] *Department of Organic and Polymeric Materials, Tokyo Institute of Technology, 2-12-1-S8-42 O-okayama, Meguro-ku, Tokyo 152-8552, Japan*

[2] *Chemistry Department, Warsaw University, Al. Zwirki i Wigury 101, 02-089 Warsaw, Poland*

[3] *Department of Physics, Faculty of Natural Sciences and Mathematics, University of Maribor, Koroska 160, 2000 Maribor, Slovenia*

[4] *Jozef Stefan Institute, Jamova 39, 1000 Ljubljana, Slovenia*

[5] *Department of Physics and Technology, Faculty of Education, University of Ljubljana, Kardeljeva ploščad 16, 1000 Ljubljana, Slovenia*

[6] *Department of Chemistry and Biochemistry, Liquid Crystal Materials Research Center, University of Colorado, Boulder, Colorado 80309-0215, USA*

[7] *Department of Physics, Liquid Crystal Materials Research Center, University of Colorado, Boulder, Colorado 80309-0390, USA*

Ferroelectric behavior in the recently reported orthogonal ferroelectric SmA_dP_F phase in an unsymmetric bent-core molecule with a carbosilane terminal group was studied. The ferroelectricity of the SmA_dP_F phase was unambiguously confirmed by optical second-harmonic generation (SHG) activity in the absence of an electric field, ferroelectric response, and high dielectric strength. The long-range polar order is a consequence of weakened interlayer coupling due to the formation of carbosilane sublayers, which allows for the parallel order of dipole moments of bent-core molecules in the neighboring layers. It develops in the system gradually through the second-order phase transition from the orthogonal SmA_d phase. In the SmA_dP_F phase the strong surface anchoring results in the splay of polarization across the sample thickness. The polar surface anchoring also brings about strongly thickness dependent polar fluctuations, as proved by the dielectric measurements (Goldstone-like mode). The relaxation frequency and dielectric strength vary more than one order of magnitude with cell thickness; in particular the dielectric strength attains more than 2000 in a 25-μm-thick cell and continues to increase for thicker cells. Simple theory developed qualitatively explains the experimental results, supporting the polarization splay model proposed.

PACS numbers:

I. INTRODUCTION

Liquid crystals are a special class of materials combining long-range order typical for crystals and the fluidity typical for liquids. Such combination results in anisotropy of physical properties accompanied by pronounced susceptibility to external stimuli, e.g., electric field. The response to an electric field can be largely enhanced if the liquid crystal is ferroelectric (FE). The first liquid crystal with ferroelectric behavior was reported by Meyer *et al.* [1], who showed that molecular chirality reduces symmetry of the tilted smectic C phase sufficiently to allow for the long range polar order. The discovery of bent-core mesogens gave a new route to achieve the macroscopic polar order [2]. The bent shape of molecules restricts rotation of molecules around their long axis and leads to spontaneous correlation of molecular transverse dipole moments so the polar smectic layers are obtained. In the past decade, a large number of bent-core molecules have been synthesized and studied, but most of the phases formed by bent-core mesogens have an antiferroelectric (AF) interlayer structure, since the AF ground state is stabilized by the energetic (the system favors apolar structure) and entropic effects (interdigitation of molecular tails between the neighboring layers) [3, 4]. Walba *et al.* attempted to suppress the antiferroelectric interlayer order by introducing branched terminal chains into bent-core molecules [5]. Several bent shaped materials with FE switching were reported, having chiral alkyl chains [6, 7], oligosiloxane [8] or oligocarbosilane [9] terminal bulky groups. However, until recently ferroelectric properties were encountered only in tilted smectic phases, while the ferroelectric orthogonal smectic phase has been searched for as a promising candidate for new displays with the advantages of high response speed, high contrast, continuous gray level, and wide viewing angle [10]. In recent years, bent-core compounds showing various non-tilted smectic phases were synthesized and investigated [11–15]. Quite recently, Reddy *et al.* reported a ferroelectric property of orthogonal smectic phase consisting of bent-core molecules with a carbosilane group at a terminal chain [16]. Here we present further unambiguous evidences for the ferroelectric behavior in the same compound.

*corresponding author; takezoe.h.aa@m.titech.ac.jp

II. EXPERIMENT

Phase transition temperatures were determined by differential scanning calorimetry (Pyris Diamond Perkin-Elmer) at a rate of 2 °C/min under cooling and heating runs. Texture observation and the identification of the mesophases were done using a polarizing optical microscope (Nikon, Optiphot-pol) equipped with a hot stage and temperature controller (Mettler Toledo FP 82). 2D X-ray patterns were obtained with Bruker GADDS system for a sample dropped on a substrate with one surface free. Homeotropic alignment was achieved by slow cooling of a droplet of the material on a heated plate. The incident X-ray beam was nearly parallel to the sample surface. Electro-optical and dielectric investigations were performed using glass cells of various thicknesses, having ITO electrodes and polymer layers for homogeneous alignment. The hysteresis loop was measured under standard conditions: the planar ITO cell, filled with liquid crystal, was in serial connection with a 100-nF capacitor, the voltage across the capacitor was measured with an oscilloscope. During the measurements the sinusoidal field was applied with a frequency of 878 Hz. Spontaneous polarization was calculated from the hysteresis loop. Complex dielectric permittivity was measured in a frequency range between 10 Hz and 10 MHz with the impedance analyzer (Solartron SI 1260). The measuring field was 0.3 V_{pp} and dc bias field up to 10 V was applied. Relaxation frequency and dielectric strength of the mode were obtained by fitting to the Cole-Cole formula. For second-harmonic generation (SHG) measurements a Nd:YAG laser (1064 nm, 8 ns duration, 10 Hz repetition) was used. The fundamental beam was incident at 45° to the planar cells. The SHG signal was detected in the transmission direction by a photomultiplier tube (R955, Hamamatsu) after blocking the fundamental light by IR-cut filter. The signal was accumulated by a boxcar integrator (SR-250, Stanford Research System) for 30 s.

III. RESULTS

Molecular structure and phase sequence of the studied bent-shaped mesogen W586 are given in Fig. 1(a). The unsymmetric molecule has a flexible alkoxy chain terminated with a carbosilane bulky group at one arm of the bent core and highly polar cyano group connected to the other arm. For this material directly below the isotropic phase a uniaxial orthogonal phase, SmA, [Fig. 1(b)] without spontaneous polarization emerges and undergoes transition to a polar smectic A (SmAP) phase on further cooling. The transition from apolar to polar orthogonal phase is accompanied by the appearance of pale schlieren texture in homeotropic cells [Fig. 1(c)]. Four-brush and two-brush defects are visible in the sample placed between crossed polarizers, as indicated by solid and dotted circles in Fig. 1(c). The former is a disclination line with strength of ±1 related to continuous reorientation of director by 2π around the defect, which is possible to exist in polar director systems as in the present case. On the contrary, the latter is forbidden in the present system, but is attributed to "chess-board "defects [17] that could be related to discontinuous reorientation of director by 2π about the defect. In planar cells both smectic phases showed fan-shape texture. In the upper phase the fans were smooth and typical for SmA phase [Fig. 1(d)]. In the lower temperature smectic phase the stripes across the fan-shape domains were observed [Fig. 1(e)], and the density of stripes increased with cell thickness [Fig. 1(e)-(g)]. Apparently stripes can be nearly suppressed by strong surface anchoring in thin cells [Fig. 1(f)].

The X-ray diffraction studies show that observed phases have layered structures with liquid-like order inside the layers, as shown in Fig. 2. The layer spacing in both phases has much weaker temperature dependence than in the SmAP_R phase [15]. The lower temperature orthogonal smectic phase has much better defined layers, as evidenced by larger number of harmonics of the main signal. The measured layer thickness, $d = 60.0{\sim}60.8$ Å, is considerably larger than the calculated length of the most extended, all-trans conformer, $L = 55$ Å[Fig. 2(c) inset]. This implies a partially intercalated structure of both the SmA phases (SmA_d type). The relatively small difference between d and L suggests a structure of the smectic layer in which the neighboring molecules overlap mesogenic cores but alternate, up and down, the position of their terminal carbosilane groups [Fig. 2 (d)]. Similar packing scheme of unsymmetric banana molecules was also proposed by Sadashiva *et al.* in the antiferroelectric SmA_dP_A phase [13, 18]. Two diffused maxima in the wide-angle region of X-ray diffraction patterns, at 6.5 Å and 4.5 Å, reflect the mean distances of the carbosilane end groups and the core-core distance of bent core molecules, respectively [Fig. 2(c) and (d)]. Apparently carbosilane units are self-segregated in space, into distinct sublayers. Similar asymmetric profile of the wide angle scattering has also been reported for other bent-core mesophases with either siloxane or carbosilane bulky groups [19, 20].

In order to investigate the polar order of smectic phases second-harmonic generation (SHG) measurements were carried out with and without applying bias electric field, on cooling down from the isotropic phase. In contrast to the previously reported SmAP phases, which were all SHG inactive in the absence of an external electric field [14, 21, 22], the material studied here shows small zero-field SHG signal for incident beam at 45° to cell normal in the low temperature phase (Fig. 3). This confirms non-compensated spontaneous electric polarization, thus a polar structure of the phase (SmA_dP_F) in the ground state. Applying an external electric field causes a pronounced increase of the SH signal magnitude because of the alignment of polarization vectors. Under bias electric field SH signal becomes non-zero at temperature slightly higher than T_c, since external field induces electric polar-

ization in the paraelectric SmA_d phase close to the phase transition. Shift of the phase transition temperature under an electric field is also visible by texture observation; in the homeotropic cells weak birefringence can be induced above the SmA_dP_F-SmA_d transition temperature. This is similar to the phenomena found in the SmAP_R phase [10, 21].

Ferroelectric properties of the SmA_dP_F phase were confirmed also by the observation of switching in the external electric field. The switching was bistable with a single hysteresis loop, spontaneous polarization (P_s) appeared at the SmA_d-SmA_dP_F phase transition and gradually increased with decreasing temperature (Fig. 4). By applying a triangular wave field, a single current peak at each half cycle, which is typical for the ferroelectric response, emerged in the SmA_dP_F phase after the paraelectric to ferroelectric transition. We confirmed no current peak is observed in the paraelectric SmA_d phase. The switching was accompanied by the increase of birefringence and disappearance of stripes crossing the fan-shape domains, but no changes in the extinction directions in the microscopic texture.

In order to explore both the individual and collective motions of molecules for the studied system, the dielectric dispersion measurements were performed in a broad temperature range. The real and imaginary parts of the dielectric constant are plotted against temperature and frequency in Fig. 5(a) and (b), respectively. In the paraelectric SmA_d phase, close to the transition to the ferroelectric phase, the dielectric relaxation mode originating from the cooperative motion of dipole moments emerges gradually. As the temperature is lowered in the SmA_d phase the mode relaxation frequency (f_r) decreases and its strength ($\Delta\varepsilon$) increases [Fig. 5(c)], which is typical behavior for the soft mode near Curie temperature. In the SmA_dP_F phase the dielectric response is high and its relaxation frequency is low, the mode is nearly temperature independent as expected for Goldstone-mode. Slight decrease of f_r on cooling is due to the gradual increase of viscosity. However, the observed relaxation mode in the SmA_dP_F phase strongly depends on the cell thickness; i.e., with increasing the thickness the strength of the mode almost linearly grows and the relaxation frequency decreases [Fig. 5(d)]. In a 1.6-μm-thick cell $\Delta\varepsilon$ is around 200 and in the 10.2- and 25-μm-thick cells it exceeds 1000 and 2000, respectively, which is much higher compared to almost all the reported bent-core mesogens. Similar thickness dependent $\Delta\varepsilon$ was observed in the ferroelectric chiral SmC^* phase due to the surface stabilized state [23]; for some chiral materials the dielectric constant attained $\sim$7500 in 250-μm-thick cell. However, by linear extrapolating of $\Delta\varepsilon$ for the studied material here even larger value ($\sim$20 000) is expected for this cell thickness. The effect of the dc bias field on the relaxation mode was also studied. By applying bias field it was possible to see that actually two modes contribute to dielectric response in the SmA_dP_F phase, strong Goldstone-like (phason mode) and much weaker soft (amplitude) mode. Under bias field the Goldstone-like mode is quickly quenched and thus soft mode becomes clearly visible (Fig. 6). The critical voltage, which suppresses the Goldstone-like mode was strongly thickness dependent, it decreased with increasing cell thickness, being $\sim$1.2 V μm^{-1} for a 3.3-μm cell and $\sim$0.05 V μm^{-1} for a 25-μm cell. Interestingly, while the relaxation frequency of the soft mode increases with increasing bias field the relaxation frequency of the Goldstone-like mode decreased, which is opposite to the typical behavior observed in the ferroelectric phase [21, 24].

IV. DISCUSSION

SHG, dielectric spectroscopy and electric switching experiments consistently show that a phase transition from the paraelectric to the ferroelectric phase takes place in the studied material, while the microscopic observations and the X-ray diffraction confirm the orthogonal nature of both phases. This novel phase sequence, SmA_d-SmA_dP_F, is probably a consequence of partial decoupling of the smectic layers due to the segregation of carbosilane molecular parts at the layer interface [Fig. 2(d)], as suggested in ref. [16]. Formation of carbosilane sublayers leads to ferroelectric structure by weakening the tendency to parallel alignment of banana arms of molecules from the neighboring layers (entropic effect). Tendency for parallel packing of molecular arms is usually considered as a driving force for the antiferroelectric arrangement of transverse dipole moments in the consecutive layers [16, 25–27]. The sublayer formation, visible in both smectic phases by the appearance of additional X-ray signal at high angle region, is apparently more pronounced in the SmA_dP_F phase, as evidenced by high number of harmonics of the main signal related to the layer periodicity.

Studies performed in the ferroelectric phase in planar cells show that in the ground state the polarization is not uniform across the cell thickness, as suggested by SHG measurements with and without applying an electric field. Instead, the polarization splay is enforced by surface conditions. Considering the anchoring energy and the polar effect at the material/glass boundary, one can expect that dipole moments of molecules close to the surface point either toward or out of the glass [Fig. 7(a)]. Since the two cell substrates are the same, the polarization splays between the cell edges to meet the boundary conditions, being parallel to the glass planes in the central part of the cell. Degeneracy of y-component sign of polarization leads to the formation of domains divided by defects, visible as stripes in the fan shaped texture [Fig. 1(g)]. The zero-field SH signal is observed due to both positive and negative splay domains, if the domain size is larger than the wavelength of light used for the measurements. This is actually the case, if we consider the fringes as boundaries of two splayed domains. In this case SHG is observable even if the two splay domains are equal in their areas within the laser beam spot. By

applying a sufficiently high electric field, bent molecules are reoriented to the field direction [Fig. 7(b)], which results in a significant increase in the SH signal magnitude. The critical field for polarization switching is cell thickness dependent, as the regions in which polarization is anchored by surfaces are relatively small compared to the bulk in thick cells. Moreover, the splay elastic energy density is larger in thinner cells, which makes the splayed polarization stable, whereas the splayed polarization can be easily deformed by applying an electric field in thick cells, resulting in lower critical field.

To study theoretically the spatial variation of the spontaneous polarization across the cell, we minimize the free energy. The free energy density is written in terms of the polar order parameter ($\vec{p}$) which is a unit vector in the direction of the local spontaneous polarization, i.e. in the direction in which the molecular tips are oriented. Since polarization is a real vector in bent-core LCs, terms $(\vec{\bigtriangledown}\cdot\vec{p})^i$, with $i = 1, 2, 3,...$ are allowed in the free energy density [28]. In addition we have to consider the spontaneous polarization self interaction [29] and the effect of the bias external electric field E_B. So the free energy density (f) is expressed as:

$$f = K_{p1}(\vec{\nabla}\cdot\vec{p}) + \frac{1}{2}K_{p2}(\vec{\nabla}\cdot\vec{p})^2 + \frac{P_0^2 p_x^2}{2\varepsilon\varepsilon_0} - E_B P_0 p_x, \quad (1)$$

where $\vec{p} = (p_x(x), p_y(x))$ is the polar order parameter ($|\vec{p}|$=1), P_0 is the magnitude of polarization, ε is the static dielectric constant and K_{p1} and K_{p2} are elastic constants related to the splay of polarization. The quadratic, $(\vec{\nabla}\cdot\vec{p})^2$, term is the typical splay elastic energy for distortion of the in-plane orientation field of the biaxial order. The linear, $(\vec{\nabla}\cdot\vec{p})$, term is required by the symmetry of the polar ordering, but, in such a finite planar cell, is well known to be mathematically equivalent to a surface energy $K_{p1}p_x|_{x=\pm L/2}$ [30]. The electrostatic term describes the polarization self interaction and the last term in Eq. (1) presents the coupling of polarization with the static external bias electric field. The condition for the equilibrium is given by the Euler-Lagrange equation:

$$\frac{\partial f}{\partial p_x} - \frac{d}{dx}\frac{\partial f}{\partial(dp_x/dx)} = 0 \quad (2)$$

and by the boundary conditions

$$\left[\pm\frac{\partial f}{\partial(dp_x/dx)} + \frac{\partial f_S}{\partial p_x}\right]_{x=\pm\frac{1}{2}L} = 0. \quad (3)$$

As the surfaces are the same, polarization at the bottom and upper surfaces tends to point in the opposite direction and the surface energy f_S is expressed as:

$$f_S = W_S(p_x \pm 1)^2|_{x=\pm\frac{1}{2}L}, \quad (4)$$

where W_S is the surface anchoring strength. Both the surface anchoring (Eq. (4)) and the linear polarization splay term in Eq. (1) tend to enforce polarization splay in the cell. At present we shall not discuss the effects of the possible competition between these two terms. The final polarization splay is the result of a sum of the bulk splay and surface terms, which cannot be individually distinguished in a given cell. In the modeling we assume that the spontaneous polarization splay prefers the splay with the same sign as the splay enforced by the surface anchoring and we study the effect of different surface anchoring strengths on the structure and response of the cell.

Inserting the free energy density (Eq. (1)) into the equilibrium condition (Eq. (2)) and introducing the dimensionless coordinate $\tilde{x} = x/L$ leads to:

$$\frac{d^2 p_x}{d\tilde{x}^2} - \frac{L^2}{\xi^2}p_x + \frac{E_B P_0 L^2}{K_{p2}} = 0, \quad (5)$$

where

$$\xi = \sqrt{\frac{K_{p2}\varepsilon\varepsilon_0}{P_0^2}} \quad (6)$$

is a characteristic length over which the distortion in the orientation of the molecular tips is relaxed. The solution of Eq. (5) under boundary conditions given by Eq. (3) is obtained numerically [Fig. 7(c)]. For cells with low thicknesses ($L \sim \xi$) the polar order profile across the cell is almost linear, for thick cells ($L \gg \xi$) the profile is a soliton-like. In the bias field the equilibrium polar order profile is distorted, as dipoles, i.e. the tips of the molecules, rotate towards the external electric field direction [Fig. 7(d)], so the average value of the x-component of the polar director, defined as $\langle p_x\rangle L = \int_{-\frac{1}{2}L}^{\frac{1}{2}L} p_x dx$, increases with increasing bias field. The dependence on the bias field is linear (see the inset to Fig. 7(d)).

We define the voltage across the cell at which the average value of polar order reaches $\frac{1}{2}$ as $U_{1/2}$. The plot of $U_{1/2}$ as a function of cell thickness L for three different strengths of surface anchoring W_S is shown in Fig. 8. We see that there exists some critical value of the surface anchoring ($W_S \sim 6K_{p2}/L$), below which $U_{1/2}$ increases uniformly with the cell thickness. Above this value there is anomalous behavior since $U_{1/2}$ decreases with increasing cell thickness at low cell thicknesses. If an experimental critical voltage is defined as a value at which the dielectric response under bias falls to one half of its initial value, we can compare qualitatively the experimental results (Fig. 8, inset) and theoretical predictions. Since experimentally we observe monotonic decrease of $U_{1/2}$ with increasing cell thickness, we conclude that i) we are in the regime of strong anchoring and ii) the correlation length is of the order of $\xi \sim$10 μm. As Fig. 7(d) shows, the electrical and optical response of the polarization charge stabilized splayed state with fixed boundary conditions is analog and continuous. Therefore the hysteretic current response of Fig. 4 is evidence for a field-induced surface transition in which one of the surfaces in the splayed state is flipped to the field orientation at $E \sim$several V/μm.

This transition is generally first order [31], generating the observed hysteresis. The electro-optic response is analog if the field is kept below the surface transition threshold. In ref. 16 the surface anchoring of $\vec{p}$, which was parallel to the surface, was strong enough that only analog electro-optics were observed.

To account for the dielectric response (Goldstone-like mode) of the splayed structure, fluctuations $\delta p(x,t)$ from the equilibrium value of the polar order parameter $p_0(x)$ are introduced:

$$p_x(x,t) = p_0(x) + \delta p(x,t). \tag{7}$$

The fluctuation part of order parameter can be expressed as [32, 33]

$$\delta p(x,t) = \delta p_0 \cos(q_w x) e^{-\frac{t}{\tau}}, \tag{8}$$

with τ being the characteristic time in which the system relaxes to the equilibrium state and q_w the wave number which depends on the strength of surface anchoring. The system dynamics is described by the Landau-Khalatnik equation:

$$-\gamma \frac{\partial \delta p(x,t)}{\partial t} = \frac{\partial f}{\partial p_x} - \frac{d}{dx}\frac{\partial f}{\partial (dp_x/dx)}, \tag{9}$$

where γ is the rotational viscosity. Introducing Eq. (8) into Eq. (9) gives

$$\frac{1}{\tau} = \frac{P_0^2}{\gamma \varepsilon \varepsilon_0} + \frac{K_{p2}}{\gamma} q_w^2. \tag{10}$$

Inserting Eq. (8) into the boundary condition Eq. (3) leads to the transcendental equation for q_w:

$$q_w L \tan(q_w \frac{1}{2} L) = \frac{L}{\xi_S} \tag{11}$$

where $\xi_S = K_{p2}/W_S$ is the surface extrapolation length. At very strong anchoring $\xi_S \to 0$ and $q_w L/2 \to \pi/2$. If $L/\xi_S \ll 1$ then $q_w^2 \approx 2/(L\xi_S)$. However, if the surface extrapolation length is comparable to the cell thickness, then q_w has to be calculated numerically from Eq. (11) and we do not have a simple dependence of the relaxation time on the cell thickness. The Eq. (10) also gives the relaxation frequency of the dielectric response. The dielectric response in the external sinusoidal field with frequency ω and amplitude E_0 is given by $\Delta\varepsilon = \lim_{E_0 \to 0} P_0(\delta p)_0/E_0$ and can be expressed as:

$$\Delta\varepsilon = \frac{P_0^2}{\frac{P_0^2}{\varepsilon\varepsilon_0} + K_{p2} q_w^2 - i\omega\gamma}. \tag{12}$$

Figure 9(a) gives the theoretical prediction for the relaxation frequency of the Goldstone-like mode as a function of cell thickness in the units of surface extrapolation length. The shape of the curve depends on the ratio between the surface extrapolation length (ξ_S) and the correlation length ξ. The dielectric strength is proportional to $1/f_r$ and is shown in Fig. 9(b) for three values of ξ/ξ_S. Comparing the theoretical prediction and the experimental results (inset in Fig. 9), we conclude that $\xi_S \approx 0.1\xi$ showing that surface extrapolation length is small compared to the bulk correlation length.

V. CONCLUSION

A novel orthogonal smectic phase with macroscopic spontaneous polarization is characterized through various methods. By the optical microscopy and X-ray diffraction, the non-tilted smectic system with partially intercalated structure and carbosilane groups segregated into sublayers is identified. The phase, SmA_dP_F, is SHG active even if no electric field is applied. The SmA_dP_F phase is observed below the paraelectric phase, and developing of the polar order is visible in the dielectric spectroscopy as softening of the order parameter. In the helix-free ferroelectric phase the non-zero relaxation frequency of polar fluctuation (Goldstone-like mode) is caused by splay of polarization across the sample thickness induced by relatively strong surface anchoring. Because of this, we observe large thickness dependences in the relaxation frequency, the dielectric strength, and the critical bias field to suppress the ferroelectric behavior. Simulation based on a simple theory qualitatively agrees with the experimental results mentioned above. Comparing the model and the experimental results we estimate the correlation length in bulk and surface to about 10 μm and 1 μm, respectively.

Acknowledgments

Nataša Vaupotič and Mojca Čepič acknowledge the financial support of the Slovenian Research Agency through the research program P1-0055. Lingfeng Guo would like to thank Dr. Surajit Dhara and Dr. Yoshio Shimbo for all their help and support for this work.

[1] R. B. Meyer, L. Liebert, L. Strzelecki, P. J. Keller, Phys. (France) **36**, L-69 (1975).
[2] T. Niori, T. Sekine, J. Watanabe, T. Furukawa, H. Takezoe, J. Mater. Chem. **6**, 1231 (1996).
[3] H. Takezoe, Y. Takanishi, Jpn. J. Appl. Phys. **45**, 597 (2006).

[4] R. A. Reddy, C. Tschierske, J. Mater. Chem. **16**, 907 (2006)

[5] D. M. Walba, E. Korblova, R. Shao, J. E. Maclennan, D. R. Link, M. A. Glaser, N. A. Clark, Science **288**, 2181 (2000)

[6] M. Nakata, D. R. Link, F. Araoka, J. Thisayukta, Y. Takanishi, K. Ishikawa, J. Watanabe, H. Takezoe, Liq. Cryst. **28**, 1301 (2001).

[7] S. K. Lee, S. Heo, J. G. Lee, K.-T. Kang, K. Kusazawa, K. Nishida, Y. Shimbo, Y. Takanishi, J. Watanabe, T. Doi, T. Takahashi, H. Takezoe, J. Am. Chem. Soc. 127, 11085 (2005).

[8] G. Dantlgraber, A. Eremin, S. Diele, A. Hauser, H. Kresse, G. Pelzl, C. Tschierske, Angew. Chem., Int. Ed. **41**, 2408 (2002).

[9] C.Keith, R. A. Reddy, Hahn, H.; Lang, H.; Tschierske, C. Chem. Commun. 1898 (2004).

[10] Y. Shimbo, Y. Takanishi, K. Ishikawa, E. Gorecka, D. Pociecha, J. Mieczkowski, K. Gomola, H. Takezoe, Jpn. J. Appl. Phys. **45**, L282 (2006).

[11] A. Eremin, S. Diele, G. Pelzl, H. Nadasi, W. Weissflog, J. Salfetnikolva, H. Kresse, Phys. Rev. E **64**, 051707 (2001).

[12] K. Gomola, L. Guo, S. Dhara, Y. Shimbo, E. Gorecka, D. Pociecha, J. Mieczkowski, H. Takezoe, J. Mater . Chem. **19**, 4240 (2009).

[13] (a)B. K. Sadashiva, R. A. Reddy, R. Pratibha, N. V. Madhusudana, Chem. Commun. 2140 (2001); (b)B. K. Sadashiva, R. A. Reddy, R. Pratibha, N. V. Madhusudana, J. Mater . Chem. **12**, 943 (2002).

[14] K. Gomola, L. Guo, D. Pociecha, F. Araoka, K. Ishikawa, H. Takezoe, J. Mater . Chem. **20**, 7944 (2010).

[15] L. Guo, K. Gomola, E. Gorecka, D. Pociecha, S. Dhara, F. Araoka, K. Ishikawa, H. Takezoe, Soft Mat. **7**, 2895 (2011).

[16] R. A. Reddy, C. Zhu, R. Shao, E. Korblova, T. Gong, Y. Shen, E. Garcia, M. A. Glaser, J. E. Maclennan, D. M. Walba, N. A. Clark, Science, **332**, 72 (2011)

[17] E. Demikhov, Europhys. Lett., **25**, 259 (1994)

[18] R. Amaranatha Reddy, B. K. Sadashiva, J. Mater . Chem. **14**, 310 (2004).

[19] C. Keith, R. A. Reddy, A. Hauser, U. Baumeister, C. Tschierske, J. Am. Chem. Soc. **128**, 3051 (2006).

[20] C. Keith, G. Dantlgraber, R. A. Reddy, U. Baumeister, M. Prehm, H. Hahn, H. Lang, C. Tschierske, J. Mater . Chem. **17**, 3796 (2007).

[21] Y. Shimbo, E. Gorecka, D. Pociecha, F. Araoka, M. Goto, Y. Takanishi, K. Ishikawa, J. Mieczkowski, K. Gomola, H. Takezoe, Phy. Rev. Lett. **97**, 113901 (2006).

[22] L. Guo, S. Dhara, B. K. Sadashiva, S. Radhika, R. Pratibha, Y. Shimbo, F. Araoka, K. Ishikawa, H. Takezoe, Phys. Rev. E **81**, 011703 (2010).

[23] M. Ozaki, K. Yoshino, T. Sakurai, N. Mikami, R. Higuchi, J. Chem. Phys. **86**, 3648 (1987).

[24] E. Gorecka, D. Pociecha, F. Araoka, D. R. Link, M. Nakata, J. Thisayukta, Y. Takanishi, K. Ishikawa, J. Watanabe, H. Takezoe, Phys. Rev. E **62**, R4524 (2000).

[25] Y. Takanishi, A. Ikeda, H. Takezoe, A. Fukuda, Phys. Rev. E **51**, 400 (1995).

[26] K. -H. Kim, K. Ishikawa, H. Takezoe and A. Fukuda, Phys. Rev. E **51**, 2166 (1995).

[27] M. A. Glaser and N. A. Clark, Phys. Rev. E **66**, 021711 (2002).

[28] D. A. Coleman, J. Fernsler, N. Chattham, M. Nakata, Y. Takanishi, E. Korblova, D. R. Link, R.-F. Shao, W. G. Jang, J. E. Maclennan, O. Mondainn-Monval, C. Boyer, W. Weissflog, G. Pelzl, L.-C. Chien, J. Zasadzinski, J. Watanabe, D. M. Walba, H. Takezoe, N. A. Clark, Science **301**,1204 (2003).

[29] M. Čopič, J. E. Maclennan, N. A. Clark, Phys. Rev. E **65**, 021708 (2002).

[30] M. A. Handschy, N. A. Clark and S.T. Lagerwall, Phys. Rev. Lett. **51**, 471-474 (1983).

[31] M. A. Handschy, N. A. Clark, S. T. Lagerwall, Phys. Rev. Lett. **51**, 471 (1983)

[32] A.Rastegar, I. Muševič, M. Čopič, Ferroelectrics **181**, 219 (1996).

[33] M. Škarabot, S. Kralj, R. Blinc, I. Muševič, Liq. Cryst. **26**, 723 (1999).

FIG. 1: (Color online) (a) Molecular structure and phase sequence for compound W586. The transition temperatures are taken from DSC cooling run. (b), (c) Homeotropic textures of SmA_d and SmA_dP_F, respectively. In SmA_d, uniaxial nature is clearly observed (b), whereas two- and four-brush defects are seen in SmA_dP_F, as indicated by dotted and solid circles, respectively (see text). (d), (e) Planar textures in the SmA_d and SmA_dP_F phases, respectively, in a 10.2-μm cell. (f), (g) Planar textures in the SmA_dP_F phase in 3.3-μm and 25-μm cells respectively. Stripes across fan-shape domains are visible for thicker cells.

FIG. 2: (Color online) 2D X-ray diffraction patterns obtained for an aligned sample (a) in the SmA_d phase at 150 °C and (b) in the SmA_dP_F phase at 120 °C. (c) X-ray intensity in SmA_d and SmA_dP_F phases as a function of 2θ obtained by integration of above patterns over azimuthal angle. The wide angle signal is composed of two peaks (arrows) with maxima corresponding to 6.5 Å and 4.5 Å. Model of molecule in most extended conformation is also shown. (d) Model of the layer structure in the SmA_dP_F phase. Layer spacing $d$and molecular length L are also shown.

FIG. 3: (Color online) (a) SHG intensity as a function of temperature, measured in ground state (red circles) and under dc field for 10 V (black squares). A 4.7-μm-thick rubbed planar cell was used in this measurement. .

FIG. 4: Spontaneous polarization, P_s, as a function of temperature. The hysteresis loop recorded at 125 °C is also shown in the inset, indicating the bistable ferroelectric switching.

FIG. 5: (a), (b) Frequency and temperature dependences of the real and imaginary parts of the complex dielectric permittivity, respectively, measured on cooling in a 10.2-μm planar cell. (c) Relaxation frequency (f_r) and dielectric strength ($\Delta\varepsilon$) vs. temperature obtained by fitting dielectric data to Cole-Cole formula. (d) Cell thickness dependence of relaxation frequency and dielectric strength of the Goldstone-like mode in SmA_dP_F phase. The curves are guides for the eyes.

FIG. 6: The imaginary part of dielectric permittivity in the SmA_dP_F phase at 125 °C measured under bias electric fields. External field suppresses easily the phason (Goldstone-like) mode (marked as "PM"), making higher frequency amplitudon (soft) mode (marked as "AM") visible. Note that with applying bias field phason mode moves to lower frequencies.

FIG. 7: (Color online) (a) Molecular model of polarization splay structure of SmA_dP_F in a planar geometry in the ground state. (b) Polarization switches under application of an electric field. (c) Spatial variation of the x-component of the polar order parameter (p_x) across the cell (x) in units of the characteristic length (ξ) in the case of strong surface anchoring at $L/\xi = 1$ (solid line), $L/\xi = 5$ (dotted line) and $L/\xi = 15$ (dashed line). (d) Spatial variation of the order parameter component p_x at different strengths of the bias field (E_B) at strong surface anchoring and $L/\xi = 15$. Dashed line: $E_B = 0$, solid lines from bottom up: $E_B = 0.5E_{1/2}$, $E_B = E_{1/2}$, $E_B = 2E_{1/2}$. The inset: the average x-component of the polar order parameter $\langle p_x \rangle$ as a function of the bias field E_B. The field $E_{1/2}$ is chosen as a field at which $\langle p_x \rangle = 0.5$.

FIG. 8: The voltage $U_{1/2} = E_{1/2}L$ vs. L/ξ at weak surface anchoring $W_S = 0.1K_{p2}/L$ (solid line) and at infinitely strong anchoring (dashed line); the dotted line presents the dependence at $W_S = 6K_{p2}/L$ which is just above the critical value of surface anchoring; below this value the dependence of $U_{1/2}$ shows a uniform increase with increasing cell thickness. In all cases: $K_{p1}L/K_{p2}$=1. The inset: Experimental results for $U_{1/2}$ vs. L, with $U_{1/2}$defined as the voltage at which the dielectric response falls to half its value in zero field.

FIG. 9: (a) Relaxation frequency (f_r) of the dielectric response as a function of cell thickness at different ratios between the surface extrapolation length ξ_S and the bulk correlation length ξ. The inset: experimental results. (b) The dielectric strength $\Delta\varepsilon$ as a function of L/ξ_S at different ratios ξ/ξ_S. The inset: experimental results. Both graphs: solid line: ξ/ξ_S=10; dashed line: ξ/ξ_S =3; dotted line: ξ/ξ_S =1. The theoretical values of frequency and the dielectric response are scaled so that the dependencies at different ratios ξ/ξ_S can be shown on the same graph. (Dash lines in the insets are guide to eyes.)

(a)

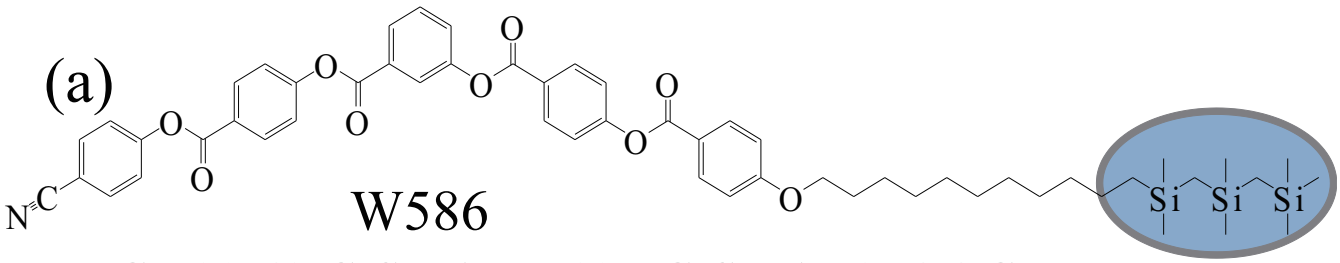

W586

Cr.-92.61°C-SmA_dP_F-137°C-SmA_d-156.6°C -Iso.

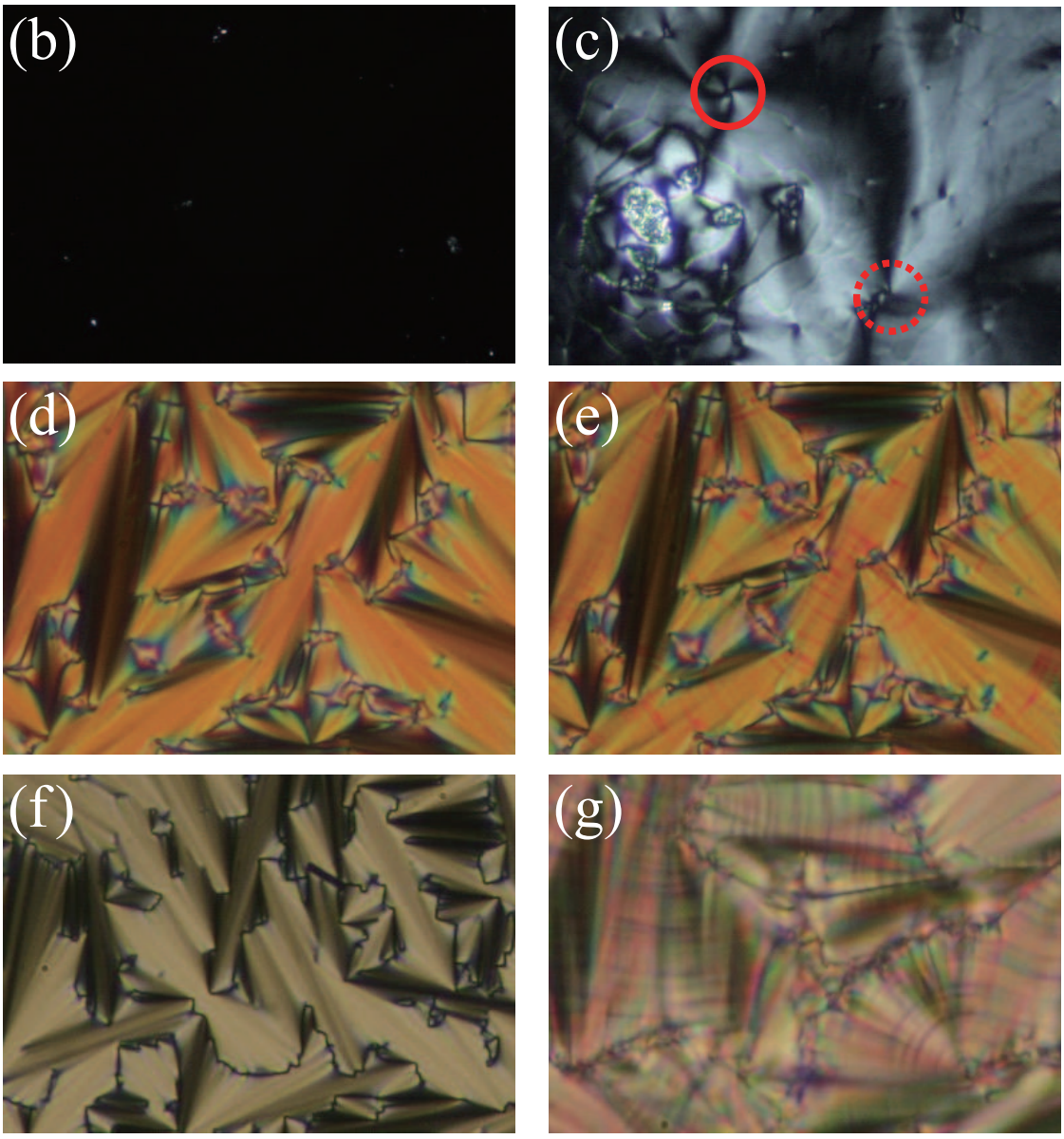

Figure 1 EG10791 30Aug2011

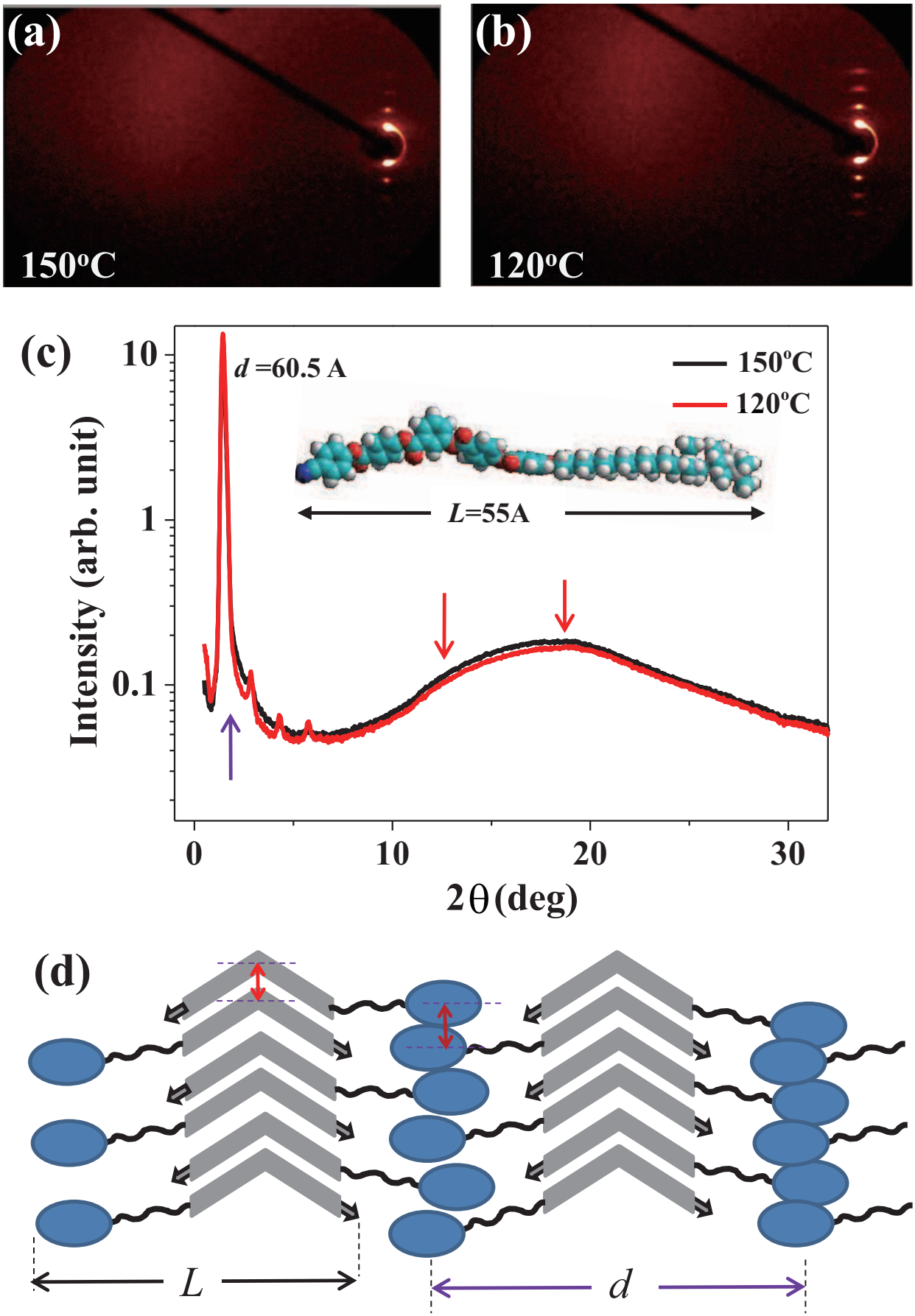

Figure 2 EG10791 30Aug2011

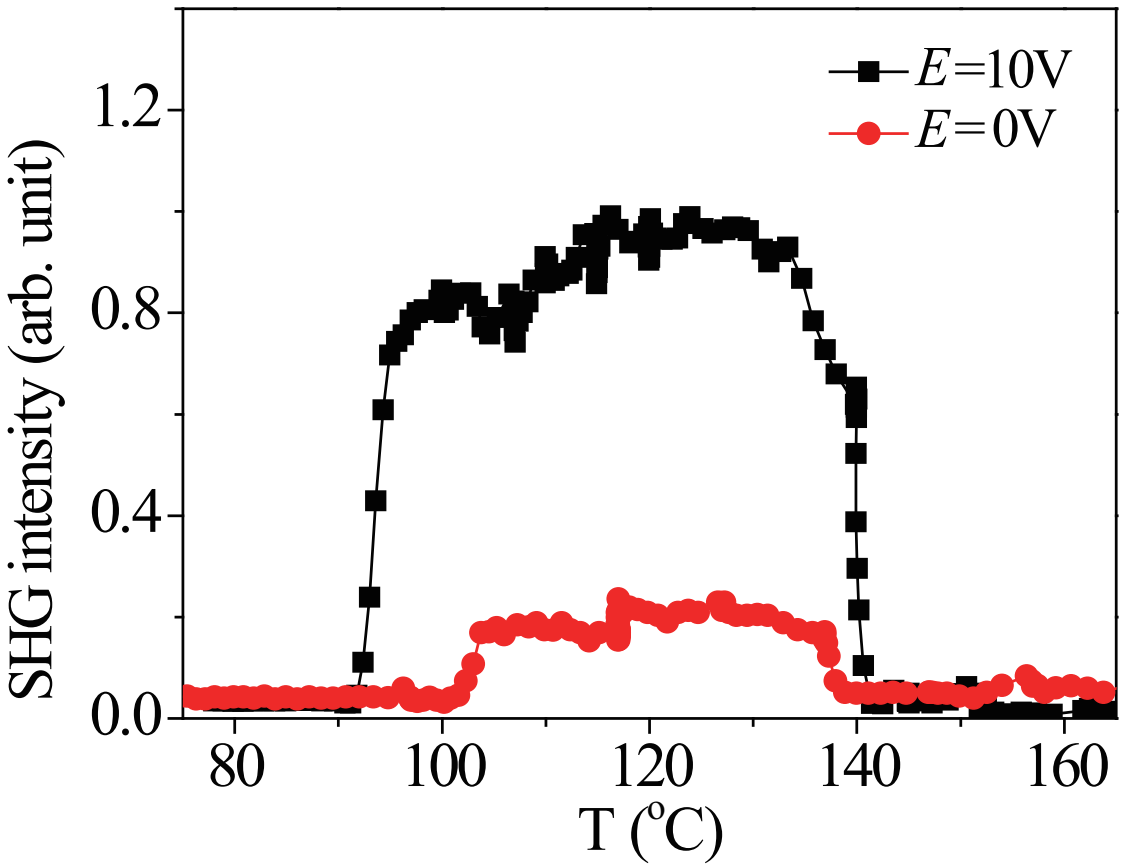

Figure 3 EG10791 30Aug2011

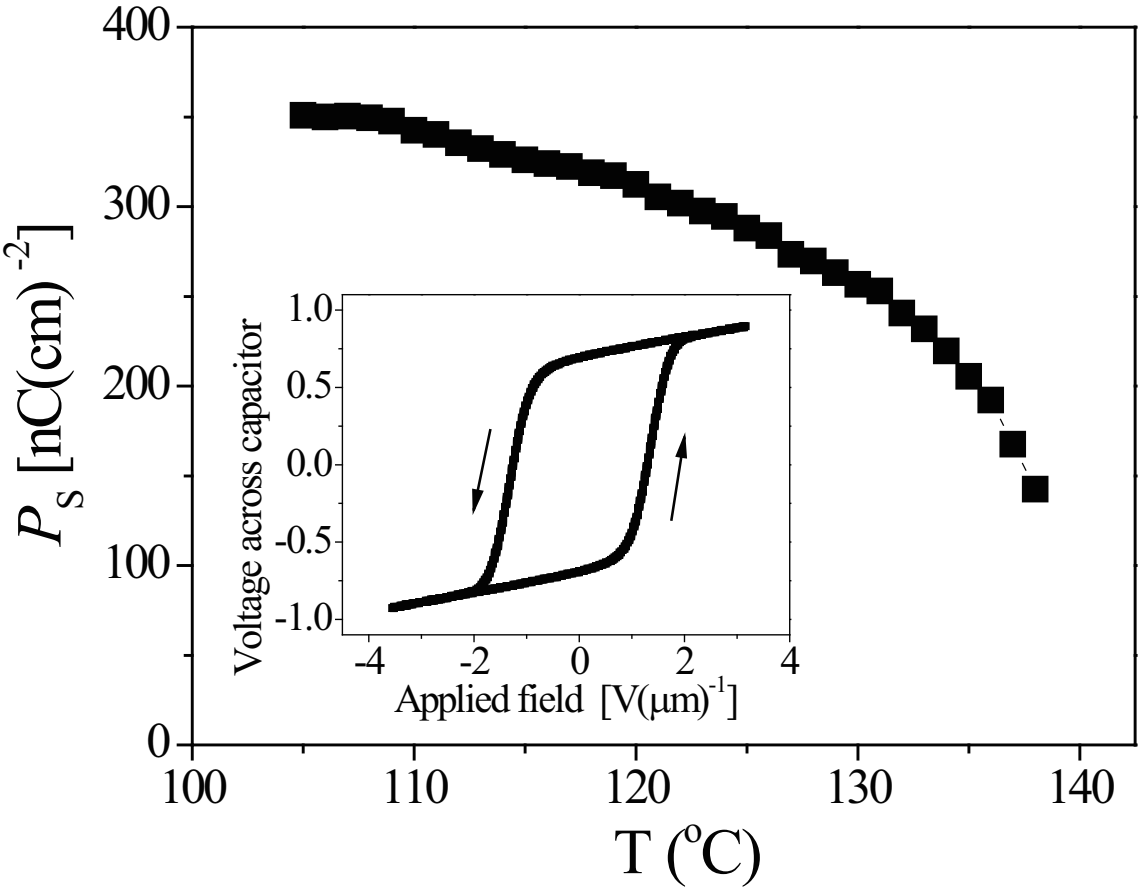

Figure 4 EG10791 30Aug2011

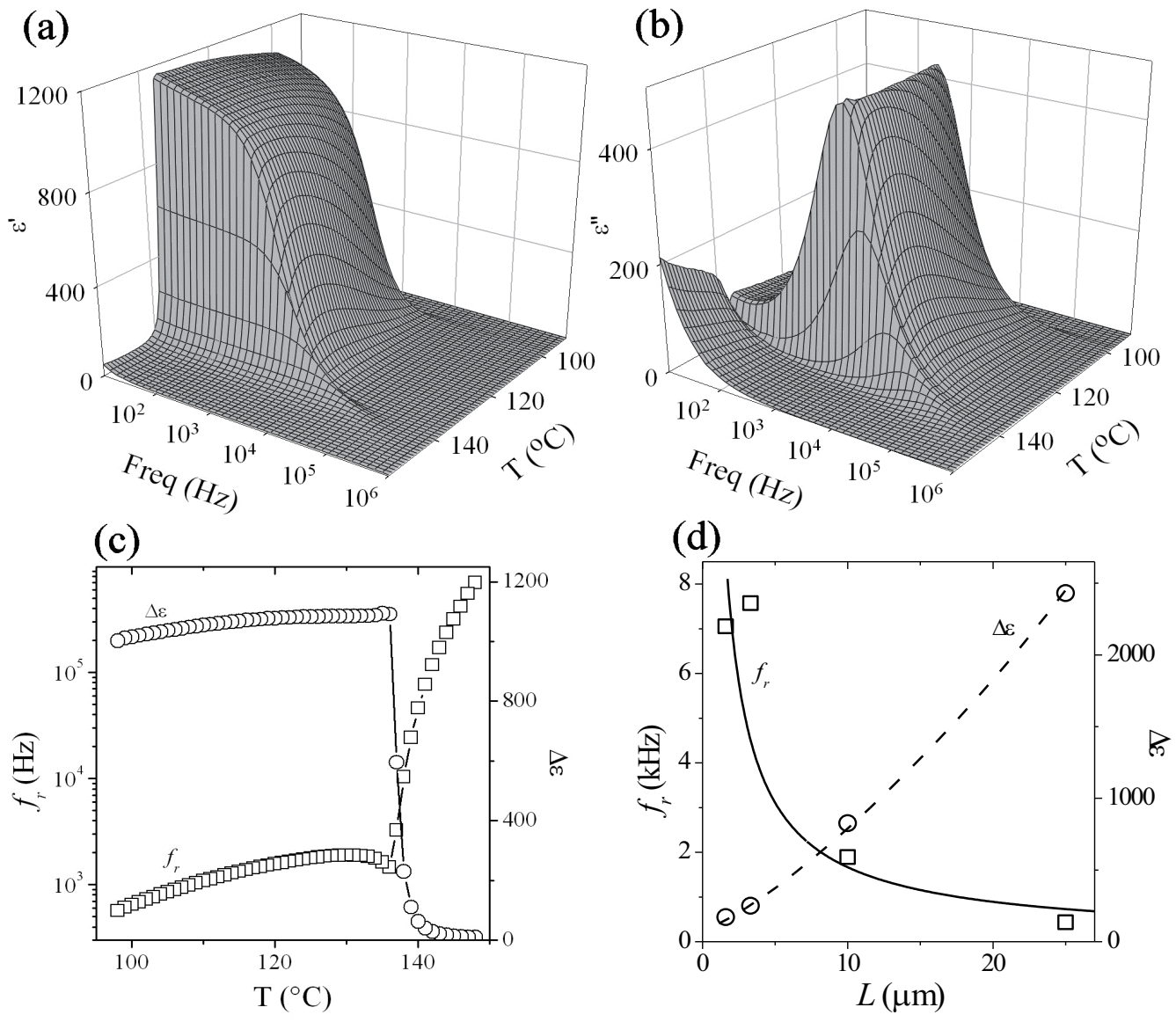

Figure 5 EG10791 30Aug2011

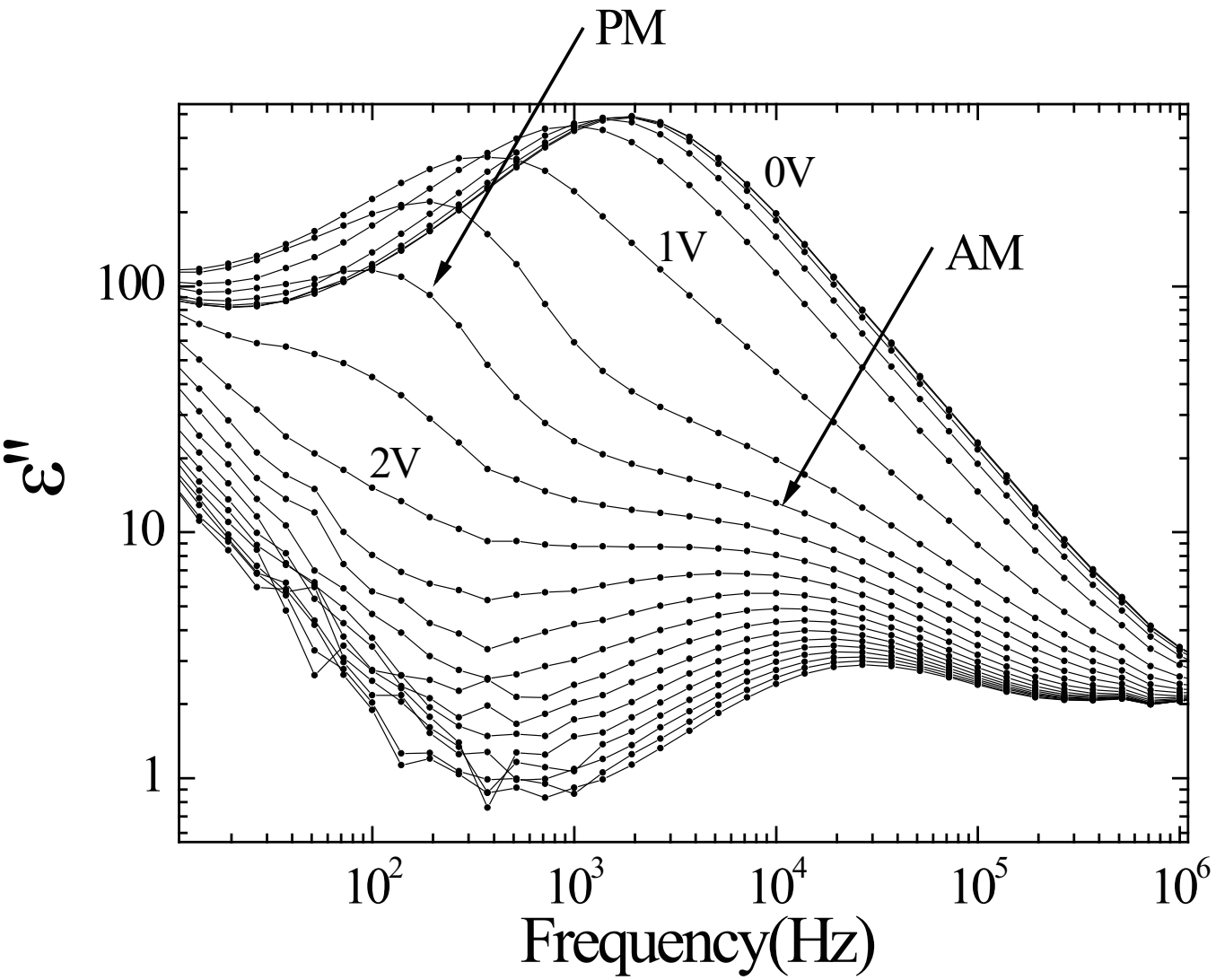

Figure 6 EG10791 30Aug2011

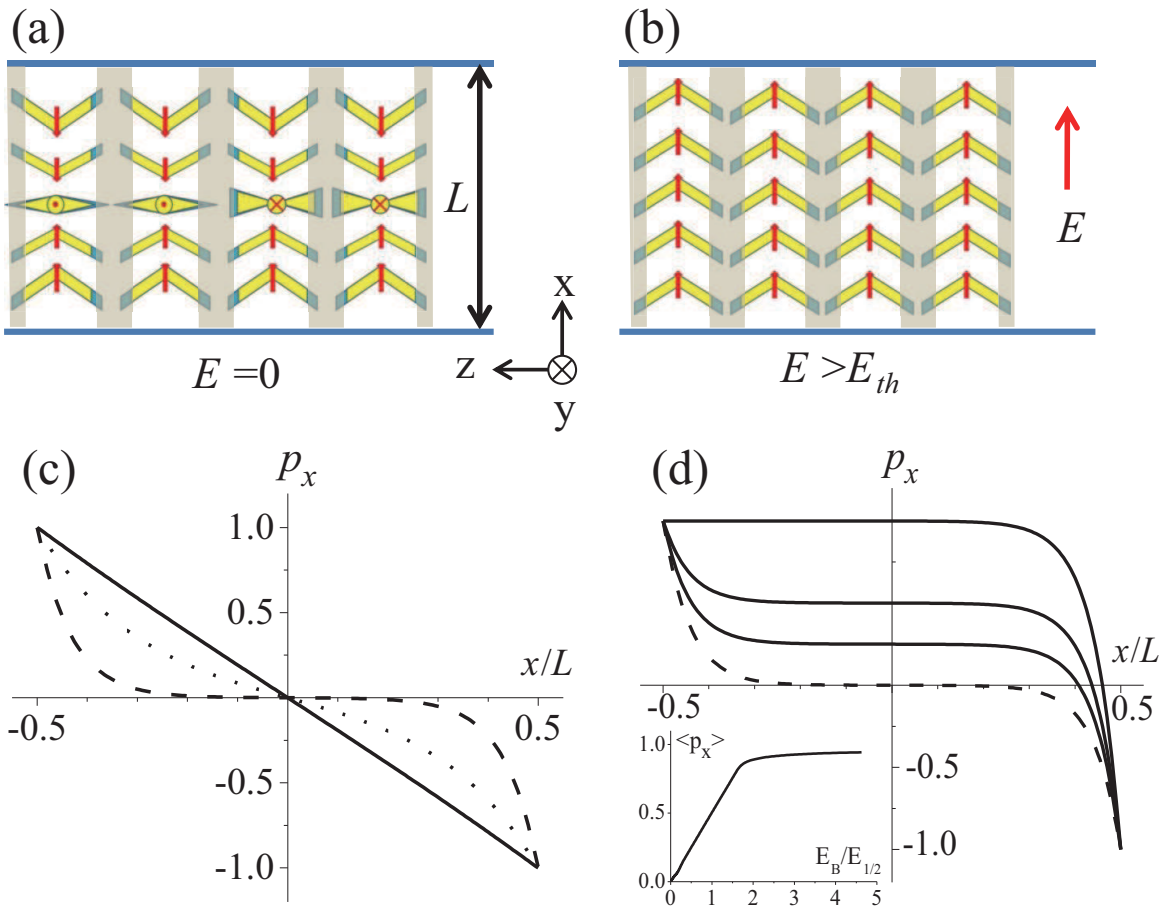

Figure 7 EG10791 30Aug2011

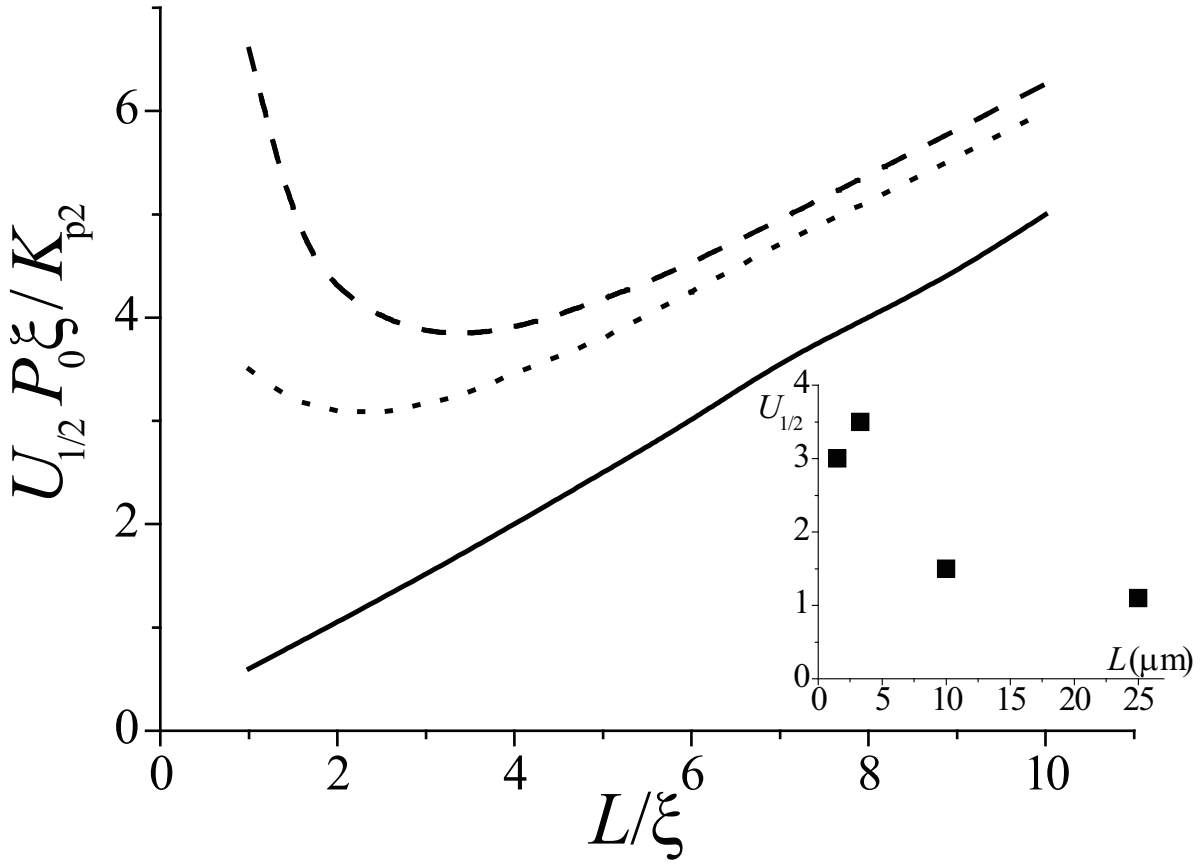

Figure 8 EG10791 30Aug2011

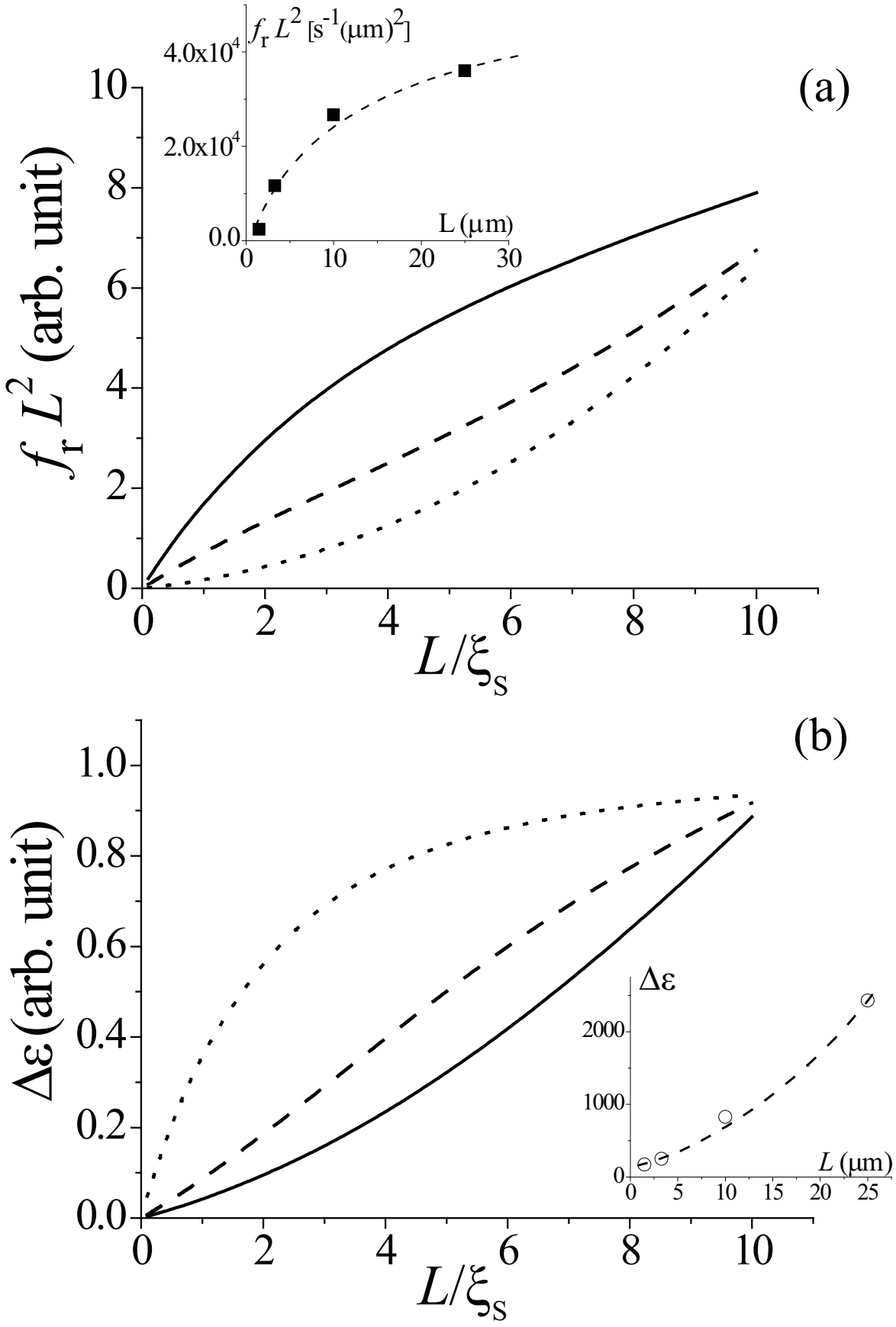

Figure 9 EG10791 30Aug2011